ROYAL SOCIETY OF CHEMISTRY

PAPER

Check for updates

Synthesising lead oxide and oxychloride minerals from spent lead acid battery waste using a choline-chloride based deep eutectic solvent

Enrico W. Manfredi-Haylock, (ID) *[a] Gwilherm K. Kerherve[a] and David J. Payne[ab]

In this study, spent lead–acid battery (LAB) paste was chemically converted into PbC_2O_4 using a choline chloride–oxalic acid deep eutectic solvent (DES). The conversion occurred at room temperature (23 ± 2 °C) within 24 h, yielding a pure PbC_2O_4 intermediate as confirmed by PXRD and XPS. Subsequent calcination produced a range of oxychloride phases depending on the temperature (300–500 °C, 1 hour) which were identified by PXRD and XPS. At 300 °C, PbC_2O_4 did not substantially decompose although yielded some traces of lead metal at the surface likely from the evolution of some CO. At 400 °C $Pb_2C_2O_4Cl_2$ and $Pb_3O_2Cl_2$ were observed in the bulk, elucidating the calcination mechanism in the presence of chlorine. Finally at 500 °C $Pb_3O_2Cl_2$ and PbO phases were obtained in the bulk with traces of oxalate remaining at the surface. Due to the room temperature nature of the conversion and the low calcination temperature, this process reduces the energy demand relative to conventional pyrometallurgy (>1000 °C) for recovering lead minerals from lead acid batteries. However, the formation of non-conductive oxychlorides presents a challenge for direct reuse in LAB manufacture. These findings highlight both the potential and limitations of if chlorine containing DES are used for battery recycling.

Sustainability spotlight

This work presents a low-energy, solvent-based process for recycling spent lead–acid batteries using a choline chloride–oxalic acid deep eutectic solvent. Unlike conventional pyrometallurgy, this method operates at room temperature for dissolution and ≤500 °C for calcination, significantly reducing CO_2 emissions and eliminating lead particulate release. The solvent is facile to synthesise, biodegradable and could enable safer, decentralised recycling suitable for deployment in low-regulation regions, thereby reducing the health burden from informal recycling. The process aligns with green chemistry principles and advances SDG 12 (responsible consumption and production) and SDG 13 (climate action).

Introduction

The impact of lead acid battery recycling

The lead acid battery (LAB) is a ubiquitous and essential piece of modern technology that allows for cheap storage of large amounts of electrical power. Starting, lighting and ignition (SLI) batteries are used in every automobile currently on the road,[1] while deep-cycle batteries are mostly used for stationary energy storage applications for electrical infrastructure.[2] Currently LABs are the most recycled product in the world with close to 100% recycling efficiency in OECD nations.[3] However there still exist two main problems with the way that LABs are currently recycled. Firstly, the dominant process (pyrometallurgy) requires smelting at >1000 °C to reduce lead materials in the spent LAB paste into metallic lead that can be resold. This

results in a process energy requirement of over 1000 kWh per tonne of lead produced. The power requirements of heating are such that fossil fuels are commonly used to power the smelter units and therefore this translates to the production of 550 kg of CO_2 per tonne of lead recycled.[4] Secondly, unless suitable emission control measures are in place, the recycling process is highly polluting and can lead to local environmental and water contamination due to lead particulate emissions. Poorly regulated recycling activities are well documented to cause health issues, particularly in developing nations where batteries are recycled informally.[5]

Innovations in lead recycling

Solution-based recycling methods have recently been gaining attention both from academia and industry. These possess the key advantages in that they do not fume lead particulates like smelting does (as all lead is trapped in solution) and typical operating temperatures of the process are around 100 °C, leading to significant energy savings. Early methods of liquid LAB recycling were based on the Betts electrowinning method[6]

[a]Department of Materials, Imperial College London, Exhibition Road, London SW7 2AZ, UK. E-mail: em2714@ic.ac.uk

[b]NEOM Education, Research and Innovation Foundation, Al Khuraybah, Tabuk, 49643-9136, Saudi Arabia

where H_2SiF_6 (hexafluorosilic acid) or HBF_4 (tetrafluoroboric acid) are used to dissolve the lead compounds. An electrostatic potential is then used to deposit pure metallic lead on the cathode. A drawback of these methods is the cost, and the chemical hazard of these powerful acids, that can evolve HF if the correct additives are not present in the solution.[7] Electrochemical processes involving less hazardous chemicals have since been developed, for example the LEDCLOR process developed by Técnicas Reunidas use mixtures of HCl and brine[8] while Aquametals Inc. have developed a methanesulphonic/ EDTA processing solution.[9] However, the drawback of all these methods is the high electrical energy consumption, which is the same or exceeding the fossil fuel equivalent of pyrometallurgy. This makes these alternative processes economically unattractive since the energy cost alone far exceeds that of traditional smelting due to the higher costing of electrical energy from the grid compared to a typical fossil fuel such as natural gas.[10]

Recently some purely chemical methods for LAB recycling have been developed to circumvent this issue. Leaching and cementation reactions have been proposed using HCl by Técnicas Reunidas (known as the PLINT process),[11] acetic acid over a metallic iron surface,[12] and citric acid.[13] These processes can either an intermediate lead product that must be calcined to lead oxide, or lead metal which must be oxidised before being used inputs for the manufacturing process of new battery active material. These products are thermally or electrochemically processed at much lower temperatures than smelting (<500 °C), yielding significant energy savings against traditional pyrometallurgy. Obtaining lead metal directly from the process has the advantages that the metal can also be used to cast the grids (after mixing with appropriate alloying elements) and the oxidation of lead metal already one of the steps on the manufacturing line, allowing for the metal product to be directly used as is. However, cementation needs another metal to be dissolved, which would lead to the process generating large amounts of waste, while electrodeposition processes to obtain lead are slow and energy intensive. Obtaining lead oxide *via* an organic intermediate requires more energy at the calcination step and directly emits CO_2, however it is often faster and therefore more energy efficient than the formation and oxidation of lead pathway in obtaining the lead oxide needed for active mass formation. The downside of all these methods outlined above is that (a) they use a lot of water in the aqueous processing solutions, (b) the chemicals used in the process for recovering lead are harmful to people and the environment and (c) the large amount of waste generated from some of these processes is not sustainable.

To tackle these three problems new chemical and electrochemical recovery method using environmentally friendly nonaqueous solvents are currently being explored[14,15] where a novel class of sustainable ionic liquid analogues known as deep eutectic solvents (henceforth referred to as DES) are used to dissolve and convert a wide variety of lead materials. Like ionic liquids, these solvents show exceptional reactivity and are able to process even stable metal oxides, but unlike ionic liquids, their synthesis is both facile and inexpensive.[16] They can also be made from commonly occurring and natural chemicals, thus making them a greener and more sustainable choice for chemical processing.[17] A common deep eutectic solvent known as Ethaline 200 is a simple mixture of choline chloride and ethylene glycol in a 1 : 2 molar ratio and is synthesised by stirring at 80 °C until it forms a colourless liquid.[18] Proof of concept work for the electrochemical recovery of lead using this solvent has been carried out for both lead perovskite materials[19] and spent LAB paste[14] and has shown promising initial results, and a new chemical process based on deep eutectic solvents is proposed.

While the above proof of concept work recovers lead electrochemically, this work proposes a new, purely chemical method of lead material recovery using a new type of DES. This DES is composed of a 1 : 1 molar ratio of choline chloride and oxalic acid dihydrate. The synthesis of this solvent is as simple and inexpensive as that of the Ethaline 200 solvent while the chemical reactivity with lead compounds is significantly higher even at room temperature. This purely chemical process yields lead(ii) oxalate which can be theoretically processed into lead(ii) oxide at less than 400 °C in 2 hours. The advantages of such a process would be (a) no electricity or heating being required to convert spent lab materials to lead(ii) oxalate (PbC_2O_4), (b) fast conversion of a mixed stream of lead compounds into a single intermediate product and (c) the circumvention of a reductive step to obtain lead metal, as this is not necessary for the manufacture of battery active material.[20]

Leaching efficiency of lead materials in this solvent was not covered in this study, as it is studied elsewhere in the literature.[21] Additionally this solvent is difficult to scale in conventional processes due to its viscosity[22] however, by tuning the properties of some solvents with water, additives or other cosolvents it may be possible to improve the speed and leaching efficiency.[23] Instead, the aim of this study was to determine what products would be produced when converting spent lead battery materials with chlorine containing DES and whether these would be useful in the manufacture of active mass for lead acid batteries. To do this, the first task of this study is to confirm the identity of the input, intermediate and output materials of this process. The input material investigated was desulphurised lead paste from spent lead acid batteries obtained from an industrial partner with unknown composition. The intermediate material and output materials require characterisation in order to elucidate the reaction and calcination mechanisms. The second task of this study was to find the lowest possible calcination temperature for the intermediate material to obtain the final useful product of lead(ii) oxide. To do this, the converted material was calcined at 300, 400 and 500 °C for one hour to observe how the temperature affects the solid state transformations of the material. All materials where characterised using XPS, XRD and SEM/EDX.

Experimental

DES preparation and reaction

The DES was prepared by mixing choline chloride (≥98%, Sigma-Aldrich) and oxalic acid di-hydrate (≥99%, Sigma-Aldrich) mixed
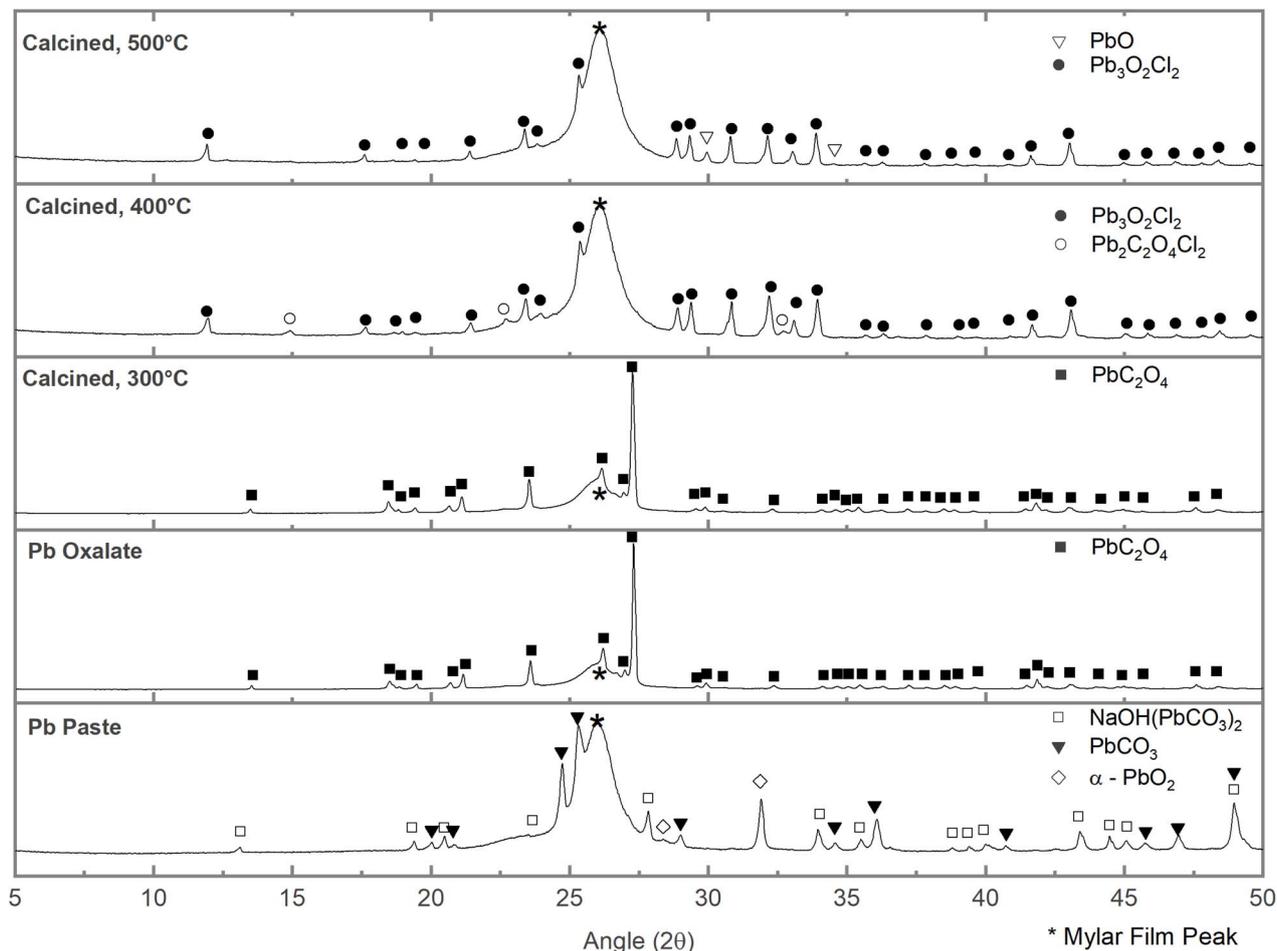
Fig. 1 XRD patterns of (bottom to top) the as provided desulphurised lead acid battery paste, the converted product after reaction with ChCl : oxalic acid DES, the product after 300 °C calcination in air, the product after 400 °C calcination in air and the product after 500 °C calcination in air. An asterisk indicates a background peak from the Mylar film used to encapsulate the sample.

in a 1 : 1 molar ratio on a heated magnetic stirring plate at 50 °C and 300 rpm until a homogeneous clear liquid is formed. 5.5 mg of desulphurised spent LAB paste (provided by Envirowales Ltd) was added per ml of DES prepared, and the solution was agitated with a magnetic stirrer set to 500 rpm at room temperature (23 ± 2 °C) for 24 hours to ensure complete conversion. A suspension is formed and 35 ml is transferred to a 50 ml conical tube and then centrifuged in an Eppendorf 5804 centrifuge for 30 minutes at 5300 rpm. The precipitate is then washed in three steps. Firstly, the supernatant is decanted, and the precipitate is re-suspended in oligo-ethylene glycol (mw ∼ 200, Sigma) and centrifuged at 5300 rpm for 30 minutes. Then the supernatant is decanted, and the precipitate is then re-suspended in distilled (19 μS cm^{-1}) water and centrifuged at 5300 rpm for 30 minutes. Lastly, the supernatant is decanted, and the precipitate is re-suspended in acetone and centrifuged at 5300 rpm for 30 minutes. After the third step the supernatant is decanted, and the precipitate is transferred to a small vial and air dried in a Büchi B-585 glass oven overnight at 140 °C. The precipitate was then calcined at 300 and 500 °C in air with a 10 °C per minute heating rate. Each sample was held at the final temperature for 1 hour in an Elite

Thermal Systems TSH12/38/250 tube furnace, using a 20 ml alumina crucible and silica tube.

Solids characterisation

The spent LAB paste, chemically converted product and calcined samples were investigated with XPS, PXRD to analyse the surface and bulk compositions respectively, while SEM was used to analyse differences in surface morphology. Compositional information of certain local points of interest on the surface were also analysed using energy dispersive X-ray spectroscopy (EDX). Image analysis of fibres in secondary electron images was conducted on ImageJ by applying a black and white threshold and edge detection to the image. Fibres exhibited charging and therefore had higher white values which were set as the threshold to ensure that only fibres were detected by the black and white masking algorithm. Additionally, only objects with an aspect ratio greater than 2 were selected for counting. The resulting detected fibres were then modelled as ellipses with the semi-major axis representing the length and semi-minor axis representing the width of the fibre.

XPS was conducted in a Thermo Fisher K-alpha high throughput system using a 180° double focussing hemispherical analyser with an area detector, 400 μm X-ray spot size using an Al-Kα cathode source. Samples were fixed as to a tantalum slide as powders through the use of conductive carbon tape. Nominal analysis chamber pressure was set to 2×10^{-8} mbar before the start of the experiment. Samples were mounted as fine powders onto a tantalum slide with carbon tape. Spectra were analysed using the integrated Avantage software suite. Tougaard backgrounds were used on all core levels and the peaks were fitted with a non-linear chi square minimisation algorithm. The energy scales were calibrated with reference to the adventitious carbon peak which was set to 284.8 eV. An ion flood gun was used to prevent sample charging.

PXRD was conducted with a Panalytical X'Pert X-ray diffractometer with standard goniometer geometry using a nickel-filtered Cu-Kα cathode source. Patterns were acquired between 5 and 50° 2θ with angular step size of 0.016° and an integration time of 20 s. Samples were mounted as fine powders into a zero-diffraction silicon disk holder covered with Mylar film to prevent sample spillage. This was found to present a significant peak at around 25° (2θ) due to its crystallinity, which is marked by an asterisk in Fig. 1. Therefore, a reference pattern for the Mylar film was collected and subtracted from the sample patterns to allow for qualitative phase analysis. Data was processed with Panalytical Highscore Plus.

SEM was conducted on a JEOL6010LA using a tungsten filament and with an integrated EDX and backscatter sensor. All images were taken with at 15 kV accelerating voltage, a working distance of 21 mm and a spot size of 40 nm. Samples were mounted as fine powders to an aluminium stub with carbon tape.

Results and discussion

Desulphurised lead acid battery paste characterisation

The starting material used in this work was desulphurised lead paste provided by Envirowales Ltd This was analysed by XRD, XPS and SEM to determine the morphology and lead compounds present. The XRD pattern for this material is shown in Fig. 1. The most significant components are α-PbO_2 (ICSD 1598175), $PbCO_3$ (ICSD 6178) and $NaOH(PbCO_3)_2$ (ICSD 261807). These products are common in lead paste that has been desulphurised in $NaHCO_3$ at high temperatures.[24]

This result is correlated by XPS measurements shown in Fig. 2. The XPS survey reports the presence of Pb, Na, O, C and Si. Two lead environments are measured in the Pb 4f core level and are attributed to $NaOH(PbCO_3)_2$ or $PbCO_3$ (ref. 25) (138.5 eV) and PbO_2 (137.3 eV) respectively. The single Na environment in the Na 1s core level at 1072.2 eV is attributed to $NaOH(PbCO_3)_2$. A single Si environment in the Si 2p at 102.7 eV is attributed to SiO_2.[26] The O 1s core level was found to have three resolvable environments and these are assigned to SiO_2 (532.8 eV),[26] $NaOH(PbCO_3)_2$/$PbCO_3$ (531.4 eV)[25] and PbO or adventitious organic C–O (529.6 eV).[27] The C 1s core level was found to have 3 environments assigned to C–C (set to 284.8 eV), C–O (286.5 eV) and C=O (289.2 eV), the first of which can be
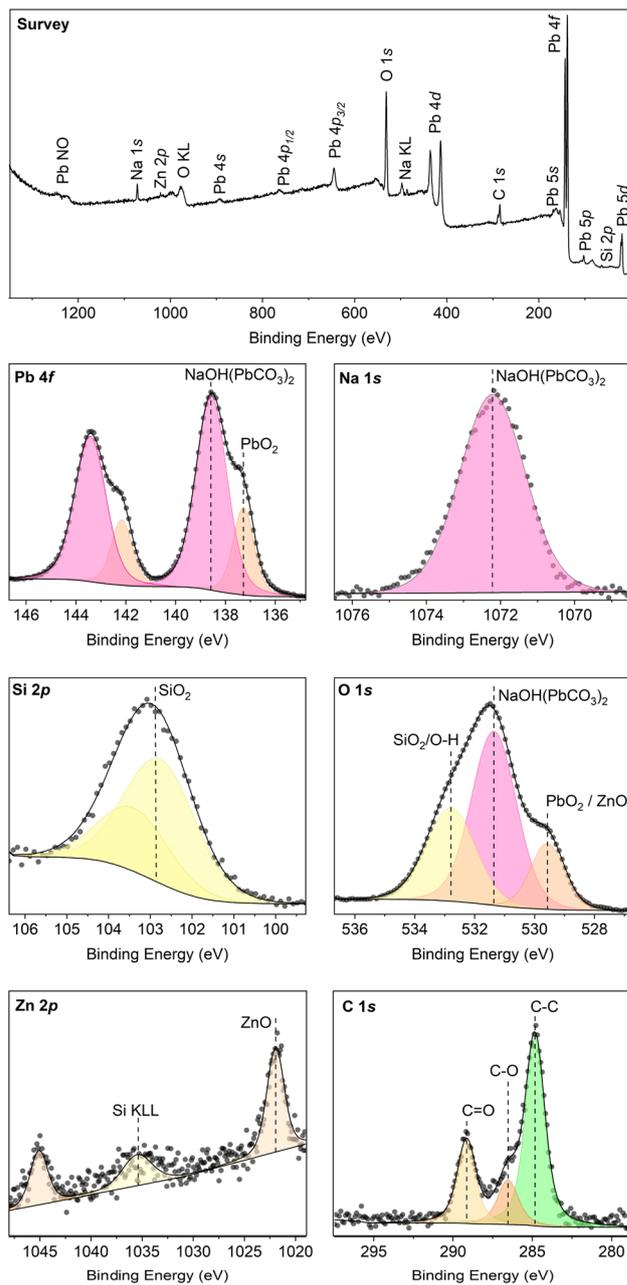

Fig. 2 XPS survey and Pb, O, Na and Si core levels for the desulphurised lead acid battery paste material.

assigned to adventitious carbon compounds (and therefore is used as an energy reference) and the latter two which are assigned to lead carbonate. The integrated peak areas of environments relating to $NaOH(PbCO_3)_2$ in the Na 1s, Pb 4f and O 1s core levels were found to be in a 1 : 2.1 : 7.2 ratio respectively. The integrated peak areas of the environments relating to SiO_2 in the Si 2p and O 1s core levels were found to be in a 1 : 2.6 ratio, which only deviates slightly from expected stoichiometry. This deviation may be due to surface hydroxyl groups because of exposure to strongly alkaline conditions during the desulphurisation process. The integrated peak areas of environments related to PbO_2 in the Pb 4f and O 1s core levels were found to be
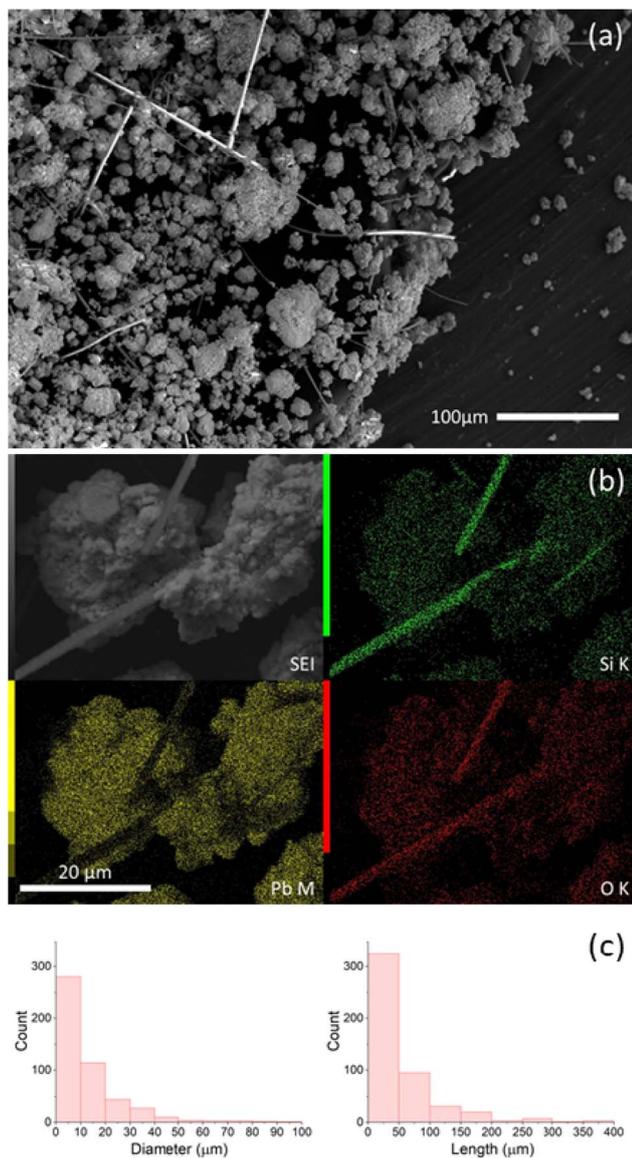
Fig. 3 (a) Low magnification secondary electron image of the desulphurised paste surface and (b) EDX area map and secondary electron image of fibres and (c) histograms of fibre length and diameter measured in SEM.

in a 1 : 3.2 ratio which deviates from the expected 1 : 2 stoichiometry. From the survey spectrum a Zn 2p environment is also seen and therefore the presence of ZnO which manifests in a similar range to PbO_2 O 1s environments at ~530.5 eV.

In SEM, large aggregates of material and bright streaks were observed (see Fig. 3a). The latter appeared to be fibres. These morphological features were investigated by EDX on the same electron microscope in Fig. 3b. It can be seen from these results that there is a strong spatial correlation between the aggregate material and the Pb M characteristic X-ray signal. Meanwhile the fibres show a positive spatial correlation with Si K and O K signal and an inverse spatial correlation with the Pb M signal. With reference to the XPS measurements, we can consider these fibres as SiO_2. The fibres were further size classified, and the results of this classification are shown in Fig. 3c. Both the

length and diameter of the fibres show a log-normal distribution from the smallest size of 10 μm diameter and 50 μm in length to the largest of 100 μm in diameter and 400 μm in length. These likely come from adsorbed glass mat (AGM) batteries that use woven silica fibres to immobilise the acid electrolyte.[28] Silica fibres from these batteries are difficult to separate from battery paste material during flotation and this indicates that AGMs make up a proportion of the batteries recycled in the batch of provided LAB paste.

Chemical conversion of paste

Once spent LAB paste is added to the DES, paste granules transform into a white suspension over 24 hours of mixing. After this a fine white powder is obtained once the precipitate is cleaned and dried. PXRD (see Fig. 1) and XPS (see Fig. 4a) analyses confirm the product is PbC_2O_4 (lead oxalate, ICSD 109830). XPS analysis shows that the Na signal is not observed in this survey scan, and very different environments are present in the O 1s, C 1s and Pb 4f core levels. A Pb metal environment (at 136.5 eV) is now present in the Pb 4f core level, the only other environment present is at 138.79 eV which is typical of organic lead compounds.[29] A dominant O 1s environment at 531.7 eV can be associated to this organic lead compound, and the only other O 1s environment at 533.4 eV is likely from SiO_2, since the Si 2p core level position remains unchanged compared to the input material. Finally, the C 1s peak associated with C=O at 288.54 eV is much more intense than the LAB paste measurement and is even more intense than the C–C peak at 284.8 eV. Therefore, since this environment's signal is more intense than that of adventitious carbon compounds, it is assumed that this environment is part of the organic lead compound formed in this product. The Pb 4f : C 1s : O 1s ratio was found to be 1 : 2.3 : 4.6, in reasonable agreement with the PXRD identification of PbC_2O_4 as the product. The powder was also imaged (shown in Fig. 4b) by SEM, and the crystal shape was noted to be plate-like with many crystal platelets sitting atop one another. This stacking of crystals is also observed in the PXRD measurement from the very high intensity of the 23.54° 2θ peak. This peak corresponds to the (002) plane of triclinic PbC_2O_4 crystals, and therefore suggests that crystal platelets preferentially align in the z direction (i.e. normal to the sample surface), as is seen in SEM.

Calcination

After being calcined at 300 °C, a grey powder was recovered. PXRD analysis (see Fig. 1) and SEM (see Fig. 5b) show the sample to be effectively unchanged compared to the original product of chemical conversion. Some subtle differences in peak intensities suggest that crystal alignment and packing has been disturbed by the calcination process. Crystals also appear to be less aligned when investigated with SEM due to some growth of small rectangular crystals between the larger platelets (shown in Fig. 5c). XPS analysis (see Fig. 5a) however shows more pronounced changes at the surface. Chlorine is detected in the survey spectrum, and a new core level is detected in the Pb 4f indicating that a chlorine-rich lead phase is formed even if
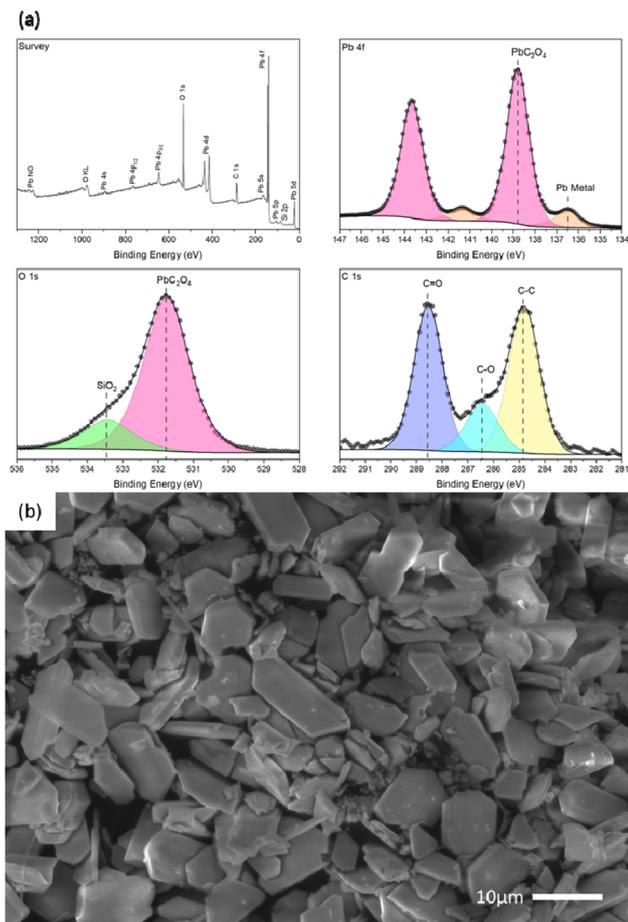
Fig. 4 (a) XPS analysis of chemically converted LAB paste showing a survey spectrum and core level spectra of Pb 4f, C 1s and O 1s. Data points of core level measurements are shown as blue dots, while the fitted environment peaks are shown as filled areas under the envelope. (b) Secondary electron image of the powder obtained after the chemical conversion of spent LAB paste.

Fig. 5 (a) XPS analysis of chemically converted LAB paste after calcination at 300 °C showing a survey spectrum and core level spectra of Pb 4f, C 1s and O 1s. Data points of core level measurements are shown as blue dots, while the fitted environment peaks are shown as filled areas under the envelope. Secondary electron images (b and c) taken at low and high magnifications respectively of the powder after calcination at 300 °C.

no change in the XRD pattern is observed compared to the freshly converted product indicating a surface reaction. The intensity ratios are taken between the Cl $2p_{3/2}$ environment at 198.05 eV and the new Pb $4f_{7/2}$ environment at 137.69 eV which are typically associated with lead chlorides and are found to be 1.79 for Cl : Pb, 1.34 for O : Cl and 1.32 for O : Pb. It should be noted that this lead core level also overlaps with PbO_2 although this is unlikely to be present as the associated Pb 4f and O 1s peaks disappear after chemical conversion. This observation could potentially be explained by the formation of mixed oxy-chloride and chloroxalate minerals which may be formed when the choline chloride component of the residual deep eutectic solvent decomposes releasing chlorine. For example, $Pb_2Cl_2C_2O_4$ and $Pb_3O_2Cl_2$ are observed in XRD at different calcination temperatures, but these may form at lower temperatures at the surface. The inference of these compounds from the ratio also indicates that all of the solid state transformations begin at the lead oxalate surface.

Even though the surface may have a highly oxidising environment, a more intense peak associated with a metallic lead
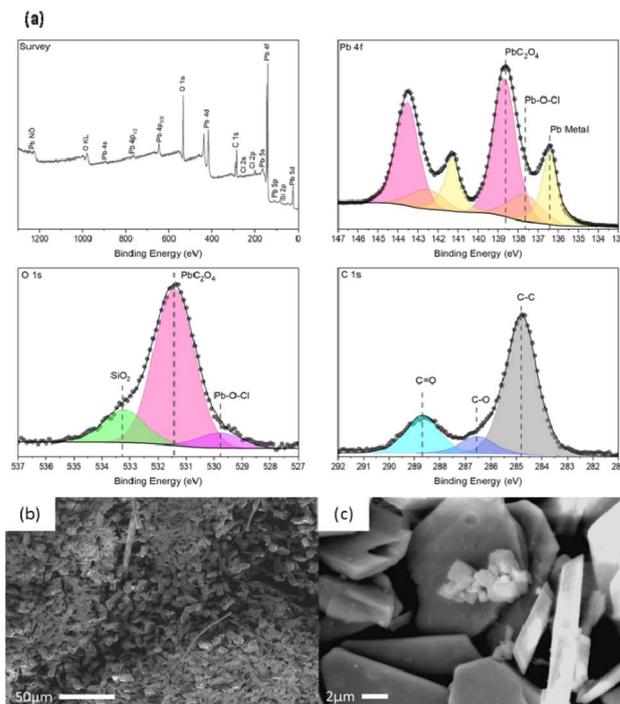
environment at 136.43 eV is also detected in the Pb 4f level at an atomic concentration of 2.6%. This environment is not detected in XRD, suggesting that this is a surface product that may be formed from the evolution of CO during the partial combustion of lead oxalate which may act as a reducing agent for the liberated lead species.[30] Even though one would expect any free lead metal to oxidise during calcination, lead's slow oxidation kinetics at 300 °C (ref. 31) makes the observation of some residual metal likely. It is noted by Boudaren *et al.* that the formation of $PbCl_2$ would also be expected at low temperatures due to the presence of some Cl_2 in the decomposition gases and its reaction with metallic lead, however this is not observed in this case, as $PbCl_2$ typically manifests at a binding energy close to 139 eV.[32]

At a higher temperatures of 400 and 500 °C a white powder is recovered after calcination and a dramatic change can be seen in PXRD (see Fig. 1), XPS and SEM (only 500 °C shown for brevity in Fig. 6a and b respectively). PXRD shows that only one phase of an oxy-chloride mineral ($Pb_3O_2Cl_2$) is present, while XPS shows a Pb : Cl ratio of 0.98 : 1 would appear to contradict the expected stoichiometry of the main phase measured by XRD. Furthermore, PbO is also measured in XRD and the shift of this Pb–O–Cl peak to 138 eV now overlaps it with the expected binding energy of PbO, which would lead to an even higher expected stoichiometry of Pb to Cl. The only way to explain a Pb : Cl ratio lower than 1 is that the chloroxalate ($Pb_2Cl_2C_2O_4$)
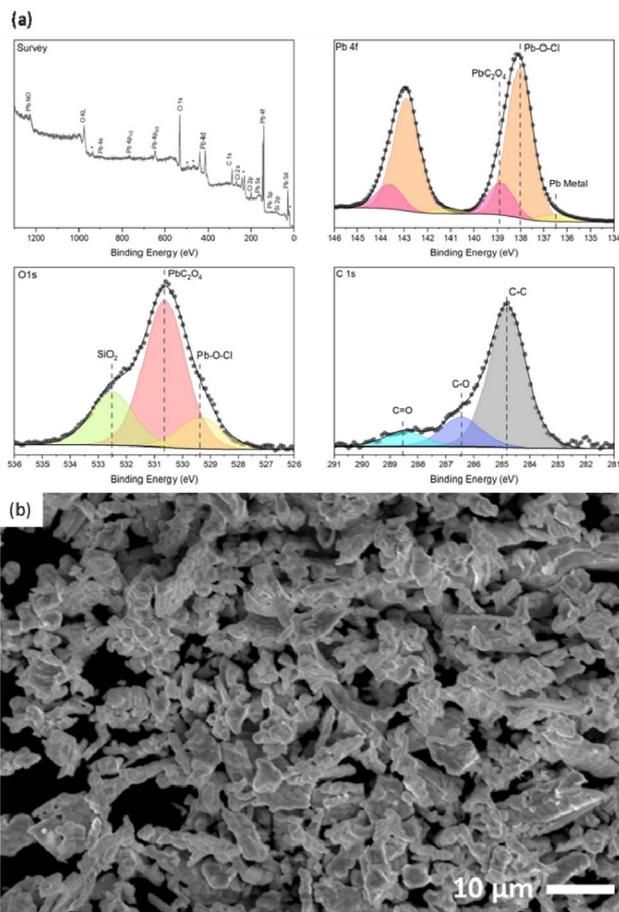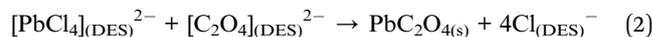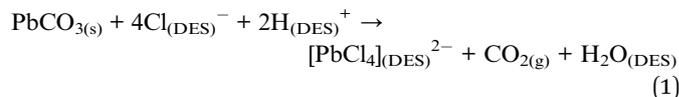
Fig. 6 (a) XPS analysis of chemically converted LAB paste after calcination at 500 °C showing a survey spectrum and core level spectra of Pb 4f, C 1s and O 1s. Data points of core level measurements are shown as blue dots, while the fitted environment peaks are shown as filled areas under the envelope. Asterisks in the survey indicate peaks contributed by the tantalum slide on which the sample was mounted. (b) Secondary electron image of the powder after calcination at 500 °C.

species identified in the bulk at 400 °C (but not at 500 °C) is still present at the surface and therefore this increases the ratio of Cl to Pb. This indicates that while the conversion from lead oxalate starts at the surface, the conversion to oxychlorides and finally lead oxide then proceeds from the bulk.

### Mechanisms of reaction and calcination

When the spent LAB paste is introduced into the deep eutectic solvent, there is an immediate reaction since some limited effervescence is observed upon addition, with a final white suspension obtained much later. The gas is likely to be CO_2 as it found to extinguish a lit wooden splint. This indicates a two-step reaction (proposed in eqn (1) and (2)) where first the lead materials are dissolved into the DES system and then react with the oxalic acid hydrogen bond donor ($C_2H_2O_4$), precipitating out of the solution. The unique chemical environment of the DES is thought to promote the availability and reactivity of the Cl anion of the choline chloride ($[C_5H_{14}NO]^+[Cl]^-$) component through a charge de-localisation that occurs between $[C_5H_{14}NO]^+[Cl]^-$ and $C_2H_2O_4$.[33] Increased Cl activity could drive

the solution of lead materials into the DES (as observed in previous studies of lead solubility in ethaline DES)[34] and consequently, $[C_2O_4]^{2-}$ can substitute the Cl^- ligands due to being a more effective chelating agent for the Pb^{2+} ion.[35]

$$PbCO_{3(s)} + 4Cl_{(DES)}^- + 2H_{(DES)}^+ \rightarrow [PbCl_4]_{(DES)}^{2-} + CO_{2(g)} + H_2O_{(DES)} \quad (1)$$

$$[PbCl_4]_{(DES)}^{2-} + [C_2O_4]_{(DES)}^{2-} \rightarrow PbC_2O_{4(s)} + 4Cl_{(DES)}^- \quad (2)$$

The identification of $Pb_2Cl_2C_2O_4$ through XRD indicates that another reaction must occur between the chlorine anion and PbC_2O_4. Since $Pb_2Cl_2C_2O_4$ was not found by XPS analysis, it was concluded that this product could form where some DES is trapped between two stacked PbC_2O_4 plates.
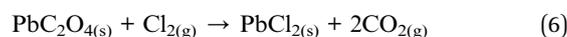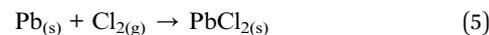
This may occur during the cleaning process, when crystals wetted with DES will flocculate due to the DES providing a more favourable surface interaction than the diluent. Prolonged exposure to the DES then leads to the surface PbC_2O_4 crystals to transform into $Pb_2Cl_2C_2O_4$ (as proposed in eqn (3)).

$$2PbC_2O_{4(s)} + 2Cl_{(DES)}^- \rightarrow Pb_2Cl_2C_2O_{4(s)} + 2CO_{2(g)} \quad (3)$$
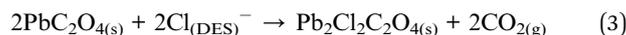
During calcination it is expected that the trapped DES would thermally degrade even at low temperatures. Generally the degradation temperature of a given DES can be estimated as the average of precursor degradation temperatures.[36] Since the decomposition of $[C_5H_{14}NO]^+[Cl]^-$ and $C_2H_2O_4$ happen at 304 °C[36] and 150 °C[37] respectively, the expected degradation temperature of solvent is around 230 °C. Hence degradation will proceed rapidly during calcination at 300 °C and the proposed stoichiometric decomposition pathway is shown in eqn (4).

$$2([C_5H_{14}NO]^+ \cdot [Cl]^- \cdot [C_2O_4]^{2-})_{(DES)} \rightarrow 14CO_{2(g)} + Cl_{2(g)} + N_{2(g)} + 14H_2O_{(g)} \quad (4)$$
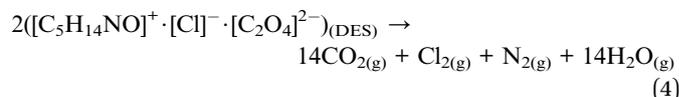
It is unlikely that the oxygen requirements for stoichiometric decomposition of the DES will be met in ambient air, therefore there may be many products of partial combustion such as CO and intermediate organic substances. As previously discussed, the former is likely responsible for the evolution of metallic lead during calcination, while the latter can confound XPS identification of the final product with overlap in the O 1s core level region. Half a mole of chlorine gas will be evolved per mole of DES decomposed and this could also drive side reactions with other calcination and combustion products. For example, the mineral mendipite can be formed by reacting PbO and $PbCl_2$,[38] where the $PbCl_2$ may be produced by a reaction between Cl_2 and metallic Pb, or PbC_2O_4 as shown in eqn (5) and (6).

$$Pb_{(s)} + Cl_{2(g)} \rightarrow PbCl_{2(s)} \quad (5)$$

$$PbC_2O_{4(s)} + Cl_{2(g)} \rightarrow PbCl_{2(s)} + 2CO_{2(g)} \quad (6)$$

As discussed by Boudaren *et al.*[30] $Pb_2Cl_2C_2O_4$ also has some thermal decomposition pathways that can lead to the formation

Table 1 Comparison of different precipitation methods for recycling lead from waste battery materials

	Placid	Fe cementation	Citrate calcination	DES calcination
Water (L kg^{-1})	2.2	20	5.0	0.0
Energy consumption	High	Low	Medium	Medium
Input	Lime, sodiumhydrosulphide	Iron, acetic acid, urea	Citric acid, H_2O_2, acetic acid	Choline chloride, oxalic acid
Waste product	Gypsum	$FeSO_4$	CO_2	CO_2
Lead form	Metal	Metal	PbO	Pb–O–Cl

of $PbCl_2$, $Pb_5O_2Cl_6$ and $Pb_3O_2Cl_2$. It is likely that the kinetics of these mechanisms are slow at temperatures of 300 °C or below, resulting in very little change as seen in the chemically converted LAB paste calcined at this temperature. However, above this temperature, significant transformations take place as is seen in the specimen calcined at 500 °C. In summary, compared to other methods in literature listed in the introduction, such as conversion and electrowinning, cementation or calcination using citric acid, this method potentially provides benefit due to not requiring any water in this process due to the solvent being a non-aqueous DES and needing fewer input chemicals to run the process (see Table 1). However, the large amounts of chlorine present in samples during thermal decomposition experiments significantly complicate the degradation behaviour, and lead to the formation of lead oxychloride products as opposed to the expected lead oxides. Further measurements and analysis are needed at intermediate temperatures to fully characterise the transformations taking place within these chemically converted spent LAB paste samples during calcination. The next steps of this study would involve varying the time and temperature of the calcinations to determine the kinetics of the solid state conversions to elucidate mechanisms that could prevent the formation of oxychlorides at lower temperatures to minimise the calcination energy consumption.

Conclusions

Spent LAB paste was converted into PbC_2O_4 using a choline chloride–oxalic acid DES within 24 h at 23 ± 2 °C. Micron sized silica fibres (mostly 0–10 μm in diameter and 0–50 μm in length, log normal distribution) were found to be present in the starting material and were also shown to persist through all process steps. Subsequent calcination at 300 °C retained PbC_2O_4 with surface Pb–O–Cl bonds detected by XPS, while calcination at 400–500 °C yielded $Pb_3O_2Cl_2$ as the dominant phase, with some $Pb_2C_2O_4Cl_2$ formed at 400 °C and some PbO formed at 500 °C in the bulk material which gives insight into the calcination mechanism. While this approach avoids high-temperature smelting (>1000 °C) and electricity-intensive electrowinning, the presence of silica fibres in the final product as well as the presence of non-conductive oxychlorides in the final product rather than lead oxide as expected means that the process as implemented in this study is not suitable for the recycling of lead acid batteries. This study highlights the potential for using DES as a more sustainable and low energy processing route, but also the potential drawbacks of using chlorine containing DES.

Further kinetic studies are needed to determine the conditions under which chlorine contamination can be eliminated, and how much additional energy this would consume.

Author contributions

E. W. Manfredi-Haylock was responsible for writing (original draft, review & editing), investigation, methodology, formal analysis and visualisation. G. K. Kerherve was responsible for formal analysis and providing resources and validation for the XPS data. D. J. Payne was responsible for conceptualization, funding acquisition, supervision and writing (review & editing).

Conflicts of interest

There are no conflicts to declare.

Data availability

All data will be provided upon request.

Supplementary information (SI) is available. See DOI: https://doi.org/10.1039/d5su00444f.

Acknowledgements

Notes and references

1 S. Parissien, *The Life of the Automobile : a New History of the Motor Car*, Atlantic Books, 2013.
2 G. J. May, A. Davidson and B. Monahov, *J. Energy Storage*, 2018, **15**, 145–157.
3 International Lead Association, *Lead Recycling*, https://www.ila-lead.org/UserFiles/File/FS_Recycling.pdf, accessed 19 April 2019.
4 A. J. Davidson, S. P. Binks and J. Gediga, *Int. J. Life Cycle Assess.*, 2016, **21**, 1624–1636.
5 B. Schaddelee-Scholten and J. Tempowski, *Used Lead Acid Battery Recycling Health Considerations*, 2017.
6 A. Betts, *US Pat.*, US679824A, 1901.
7 R. David Prengaman, *JOM*, 1995, **47**, 31–33.

8 J. L. Alvarez, E. Hermana, D. Martin and F. Martin, in *Edited Proceedings Tenth International Lead Conference*, 1990, pp. 156–164.

9 S. R. Clarke, R. L. Clarke and B. Dougherty, WO2016183429, 2016.

10 D. Helm, *Cost of Energy Review*, 2017.

11 D. Andrews, A. Raychaudhuri and C. Frias, *J. Power Sources*, 2000, **88**, 124–129.

12 M. Volpe, D. Oliveri, G. Ferrara, M. Salvaggio, S. Piazza, S. Italiano and C. Sunseri, *Hydrometallurgy*, 2009, **96**, 123–131.

13 D. Yang, J. Liu, Q. Wang, X. Yuan, X. Zhu, L. Li, W. Zhang, Y. Hu, X. Sun, R. V. Kumar and J. Yang, *J. Power Sources*, 2014, **257**, 27–36.

14 A. D. Ballantyne, J. P. Hallett, D. J. Riley, N. Shah and D. J. Payne, *R. Soc. Open Sci.*, 2018, **5**, 171368.

15 S. Y. Tan, D. J. Payne, J. P. Hallett and G. H. Kelsall, *Curr. Opin. Electrochem.*, 2019, **16**, 83–89, DOI: 10.1016/j.coelec.2019.04.023.

16 A. P. Abbott, G. Capper, D. L. Davies, K. J. McKenzie and S. U. Obi, *J. Chem. Eng. Data*, 2006, **51**, 1280–1282.

17 A. Prabhune and R. Dey, *J. Mol. Liq.*, 2023, **379**, 121676.

18 A. P. Abbott, G. Frisch, J. Hartley, W. O. Karim and K. S. Ryder, *Prog. Nat. Sci.:Mater. Int.*, 2015, **25**, 595–602.

19 C. G. Poll, G. W. Nelson, D. M. Pickup, A. V. Chadwick, D. J. Riley and D. J. Payne, *Green Chem.*, 2016, **18**, 2946–2955.

20 D. Pavlov, in *Lead-acid Batteries: Science and Technology*, Elsevier, 2017, pp. 245–273.

21 P. Zürner and G. Frisch, *ACS Sustain. Chem. Eng.*, 2019, **7**, 5300–5308.

22 K. Binnemans and P. T. Jones, *J. Sustain. Metall.*, 2023, **9**(2), 423–438.

23 Y. Dai, G.-J. Witkamp, R. Verpoorte and Y. H. Choi, *Food Chem.*, 2015, **187**, 14–19.

24 Y. Gong, J. E. Dutrizac and T. T. Chen, *Hydrometallurgy*, 1992, **31**, 175–199.

25 J. A. Taylor and D. L. Perry, *J. Vac. Sci. Technol., A*, 1984, **2**, 771–774.

26 T. Hagio, A. Takase and S. Umebayashi, *J. Mater. Sci. Lett.*, 1992, **11**, 878–880.

27 K. S. Kim, T. J. O'Leary and N. Winograd, *Anal. Chem.*, 1973, **45**, 2214–2218.

28 H. Schulte and W. Kirchhoff, *US Pat.*, US4238557A, 1978.

29 V. I. Nefedov, Y. V Salyn and K. Keller, *Inst Obs Neorg Khimii Im Ns Kurnakova Leninski Prospekt 31, 71 Moscow, Russia*, 1979.

30 C. Boudaren, J.-P. Auffrédic, M. Louër and D. Louër, *Powder Diffr.*, 2003, **18**, 205–213.

31 G. Hope, *Aust. J. Chem.*, 1980, **33**, 471.

32 L. Montagne, S. Donze, G. Palavit, J. C. Boivin, F. Fayon, D. Massiot, J. Grimblot and L. Gengembre, *J. Non-Cryst. Solids*, 2001, **293–295**, 74–80.

33 M. R. S. J. Foreman, S. Holgersson, C. McPhee and M. S. Tyumentsev, *New J. Chem.*, 2018, **42**, 2006–2012.

34 C. G. Poll, G. W. Nelson, D. M. Pickup, A. V. Chadwick, D. J. Riley and D. J. Payne, *Green Chem.*, 2016, **18**, 2946–2955.

35 R. G. Pearson, *J. Am. Chem. Soc.*, 1963, **85**, 3533–3539.

36 F. Chemat, H. Anjum, A. M. Shariff, P. Kumar and T. Murugesan, *J. Mol. Liq.*, 2016, **218**, 301–308.

37 D. E. Wobbe and W. A. Noyes, *J. Am. Chem. Soc.*, 1926, **48**, 2856–2868.

38 O. I. Siidra, S. V Krivovichev, T. Armbruster and W. Depmeier, *Z. Kristallogr.*, 2008, **223**, 204–211.